

Article

Generalized Average Modeling of a Dual Active Bridge DC-DC Converter with Triple-Phase-Shift Modulation

Michał Rolak ^{*,†} , Maciej Twardy ^{*,†} and Cezary Soból ^{*,†}

Institute of Control and Industrial Electronics, Warsaw University of Technology, Koszykowa 75, 00-662 Warsaw, Poland

* Correspondence: michal.rolak@pw.edu.pl (M.R.); maciej.twardy@pw.edu.pl (M.T.); cezary.sobol@pw.edu.pl (C.S.)

† These authors contributed equally to this work.

Abstract: This paper shows an elaboration of an equivalent electrical circuit of a Dual Active Bridge (DAB) and its application as a versatile tool for steady-states analysis in wide range of operating conditions. This work analyses the converter which is controlled with a coherently defined Triple Phase-Shift (TPS) modulation which allows appropriate switching functions to be written, thus enabling the circuit's state-space equations to be derived. Due to this approach, a Fourier series expansion may be easily applied to utilize Generalized Averaged Modeling (GAM)—a convenient method for modeling resonant and quasi-resonant power converters. Moreover, this paper shows the utilization of the GAM model higher harmonics' complex magnitudes to calculate the steady-state power characteristics for bidirectional operation; additionally, a method for a particular state variable waveform signal reconstruction is presented. All the discussed model properties are validated with a 1.5 kW 100 kHz SiC-based DAB prototype.



Citation: Rolak, M.; Twardy, M.; Soból, C. Generalized Average Modeling of a Dual Active Bridge DC-DC Converter with Triple-Phase-Shift Modulation. *Energies* **2022**, *15*, 6092. <https://doi.org/10.3390/en15166092>

Academic Editors: Marek Adamowicz, Marek Jasinski and Kouzou Abdellah

Received: 20 July 2022

Accepted: 19 August 2022

Published: 22 August 2022

Publisher's Note: MDPI stays neutral with regard to jurisdictional claims in published maps and institutional affiliations.



Copyright: © 2022 by the authors. Licensee MDPI, Basel, Switzerland. This article is an open access article distributed under the terms and conditions of the Creative Commons Attribution (CC BY) license (<https://creativecommons.org/licenses/by/4.0/>).

Keywords: Dual Active Bridge (DAB); Triple Phase Shift Modulation (TPS); Generalized Average Modeling (GAM); power characteristics; linear time periodic system; LTP

1. Introduction

The Dual Active Bridge topology has been steadily gaining researchers' and industry's attention over the last decades. This is mainly due to its advantageous properties that may be applied to emerging power converter applications such as the much in-demand Energy Storages (ES) or Smart Transformers (ST) [1], often including Multi Modular Converters, to name just a few [2,3].

This DC/AC/DC converter operates as a quasi-resonant device assuring a lower peak current value than its resonant counterpart for the same RMS value [4]. This is possible due to the high number of the transformer's current harmonics. Moreover, this topology often offers high efficiency (usually over 97%) for significant DC voltage differences (mainly due to the utilization of a high-frequency transformer of a matched winding turns ratio) and the ability for synchronous rectification when MOSFETs are used as power switches. High efficiency may also be achieved in many operating conditions by extending the Zero Voltage Switching (ZVS) due to appropriate modulation strategies.

Despite having been the focus of research for such a long time, new problems are appearing because more demanding constraints and requirements for control algorithms and modulation techniques are needed in modern DAB applications. For instance, when the converter is used as an ES interface for grid applications, a strong need for feed-forward DC current estimation exists due to its non-linear power characteristics [5,6]. This is often a problem even for a converter that utilizes the simplest modulation of the DAB, i.e., the Single Phase-Shift modulation (SPS) [7]. On the other hand, intense research that is taking place in the field of modulation optimization aims to minimize the high-frequency transformer's RMS current [8]. This topic requires advanced modulation i.e., the Triple

Phase-Shift (TPS) [9], and may often overwhelm a reader by presenting a number of almost all possible switching states [10]. Finally, some papers such as [11] focus on obtaining exact power characteristics (as a function of a phase-shift) in order to optimize the overall efficiency of a system consisting of DAB modules connected in parallel.

To analyze and solve the described issues, two approaches are mainly used. One of them is to use advanced simulation environments where thermal libraries of power devices may be incorporated into the designed circuit. Results obtained this way are accurate but come at the cost of computation time due to the need to solve sets of Ordinary Differential Equations (ODE) numerically. On the other hand, a converter's detailed mathematical description may allow for an in-depth analysis of the examined circuit, but comes at the cost of complexity. One of the most common approaches in this latter type of modeling is to simplify the DAB topology to a single high-frequency transformer circuit which consists of two voltage sources connected in series with a lumped impedance, and allows for the derivation of general equations and basic dynamics description. This, however, ignores the parasitic components such as DC-links' ESR resistance and input/output terminals' parasitic (or designed) inductive filters. However, the detailed modeling of a DAB in this manner is justified due to the quasi-resonant nature of this topology. This undermines the validity of other popular analytical methods such as the small-ripple approximation modeling method, which is a well-known approach for basic DC/DC converters (e.g., buck, boost, flyback, etc.) [12], since the period of the high-frequency transformer's current is equal to the averaging interval.

However, due to DAB's similarity to resonant converters, the General Averaging Modeling (GAM), presented in [13] as an extension of the small-ripple approximation, may be applied. Although this approach appears in state-of-the-art papers, its treatment is fragmentary (i.e., for limited chosen state variables, or up only to fundamental harmonics) or intricate due to different TPS definitions (where often two duty-cycle and one single phase shift occur). For instance, papers such as [14–16] claim that it is sufficient to expand the model only up to the first harmonic, while [13] states that higher harmonics affect model accuracy significantly. Papers such as [5,14,17–19] consider only a few selected states variables, such as transformer current and input/output capacitor voltages, neglecting capacitors' ESR and input/output filters. It is worth mentioning that an explicit DAB equivalent circuit model is generally not presented in the GAM literature; moreover, incoherency in the TPS phase-shift definitions may result in the fact that an additional normalization procedure is required, as stated in [17].

Contribution: This paper introduces a unified DAB GAM model where the TPS is defined in a simple and coherent mathematical manner, and introduces tools for analyzing the converter in a wide range of operating conditions. This is obtained by defining a detailed electrical equivalent circuit of a DAB in the first place, describing its corresponding state-space equations, and expanding them into a Fourier series. Moreover, a simple yet accurate method based on steady-state complex magnitudes calculation is proposed for obtaining power characteristics for the TPS-controlled DAB; this is done for bidirectional energy flow and clearly demonstrates the phase-shift-drift effect, which is briefly discussed. Finally, the method presented in this paper allows us to show the model's order impact on the modeling accuracy for a wide range of operating conditions. To the authors' knowledge, none of these enumerated issues have been previously published.

The paper is organized as follows: the DAB model with its equivalent electrical circuit with state-space equations and unified TPS definition are shown in Section 2. Section 3 describes the GAM approach and its application to TPS-controlled DAB converter; the method for steady-state power characteristics is developed, and the state variable signals reconstruction from Fourier amplitudes is demonstrated. Section 4 presents the waveform reconstruction and power characteristics calculations with different GAM model orders. Finally, Section 3 presents the laboratory test bench experimental validation. Conclusions are written in Section 4.

Finally, let us note that, although it is possible to study the DAB model dynamics with the presented approach, this issue is beyond the scope of this paper and is deliberately omitted.

2. Materials and Methods

2.1. DAB Modeling

A general DAB converter topology where two DC voltage sources (V_1 and V_2) are coupled with the AC-link, is shown in Figure 1.

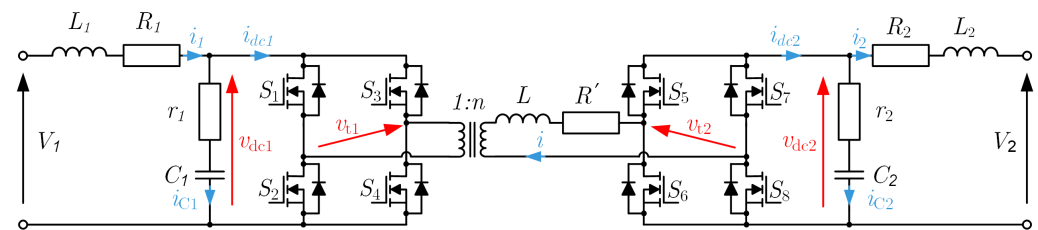


Figure 1. General scheme of the bidirectional Dual Active Bridge converter topology.

This topology consists of two H-Bridges connected via a high-frequency transformer with an n winding turns ratio. A physical auxiliary inductance (L') is connected in series with the transformer to match the power of the converter; however, it is usually lumped into a single inductance L together with the transformer's leakage inductance. Similarly, the transformer's winding resistances are combined as lumped resistance R' .

Each H-Bridge consists of 4 MOSFET switches that are grouped into two branches; thus, proper dead-times (DT) have to be applied to avoid a branch short-circuit. The DC-link capacitors (C_1 , C_2) are connected to the transistors' branches and include parasitic components such as ESRs denoted with r_1 and r_2 , respectively. These lowercase letters may be misleading, however, due to a large number of parameters in this topology. This will allow us to formulate the relevant equations in a more compact form. Finally, the V_1 , V_2 input/output circuits are modeled with a series connection of inductors containing their resistances (L_1 , R_1 and L_2 , R_2 , respectively). These values may be both a designed circuit filter or parasitic inductances and resistances of input/output terminals. Thus, the real value of voltages applied to the transformers' terminals are v_{t1} and v_{t2} which are functions of v_{dc1} and v_{dc2} multiplied by appropriate switching functions. Here, it might be mentioned that input/output terms are used interchangeably as the DAB is a bidirectional topology, where the energy flow direction changes according to the control parameter.

2.1.1. Triple-Phase-Shift Definition

The three phase-shift angles of the TPS are shown in Figure 2 where control logic signals of each power switch are presented in the top panel, and the H-bridges' ideal output voltages are shown in the bottom panel.

Thus, the phase-shifts may be defined as follows: the ϕ_1 is a phase shift between 50% duty-cycle rectangular waveforms generated at the outputs of the branches $S_1 - S_2$ and $S_3 - S_4$ whose difference makes the v_{t1} voltage; the ϕ_2 is the ϕ_1 's counterpart corresponding to branches $S_5 - S_6$ and $S_7 - S_8$ which form the v_{t2} voltage; finally the ϕ_3 is a phase-shift between v_{t1} and v_{t2} voltages. The phase shift values shown in Figure 2 are set arbitrarily to $\phi_1 = \phi_2 = \pi/2$ and $\phi_3 = \pi/3$ simply for illustration purposes. Then, a typical single SPS modulation may be simply obtained when $\phi_1 = \phi_2 = \pi$ and ϕ_3 is a control variable.

2.1.2. DAB's Electrical Equivalent Circuit

The whole DAB converter may be described by adequate subcircuits coupled with controlled current-voltage sources pairs. This is a similar approach to that which is often adopted to model typical DC/DC power converters [12]. Thus, the DAB's electrical equivalent circuit may be presented as in Figure 3, where variables i_{dc1} and v_{t1} , and i_{dc2} and v_{t2} may be modeled as controlled current-voltage sources pairs dependent on TPS

switching functions. Here, one should note that the R parameter now also includes the MOSFETs' channel resistances of both H-Bridges.

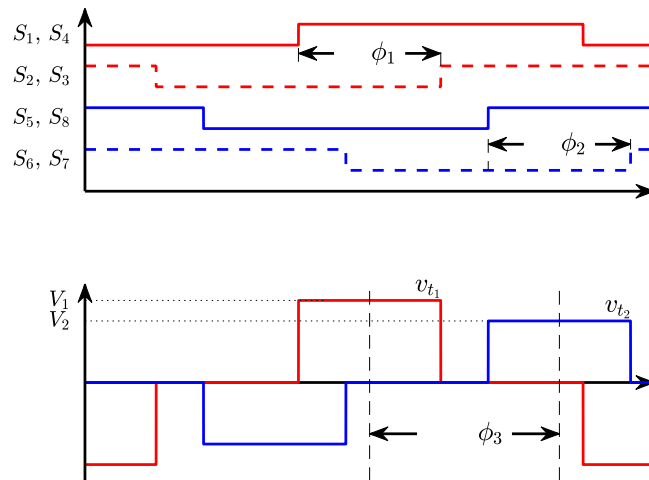


Figure 2. The TPS definition—top panel: transistors' ON/OFF control signals; bottom panel: high-frequency transformer's ideal voltages' waveforms.

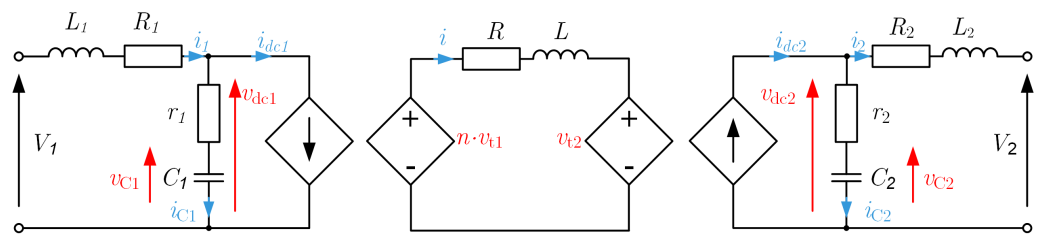


Figure 3. The equivalent electrical circuit of the DAB converter.

This representation allows for the development of a state-space model by writing the KVL, and KCL. Thus, the DAB converter may be described by a linear-time-periodic (LTP) system

$$\dot{x} = \Phi x + f, \tag{1}$$

where the time-varying matrix Φ is expressed as

$$\begin{bmatrix} -\frac{R+n^2s_1^2r_1+s_2^2r_2}{L} & \frac{ns_1r_1}{L} & -\frac{s_2r_2}{L} & \frac{ns_1}{L} & -\frac{s_2}{L} \\ \frac{ns_1r_1}{L_1} & -\frac{(R_1+r_1)}{L_1} & 0 & -\frac{1}{L_1} & 0 \\ -\frac{s_1r_2}{L_2} & 0 & -\frac{(R_2+r_2)}{L_2} & 0 & -\frac{1}{L_2} \\ -\frac{ns_1}{C_1} & \frac{1}{C_1} & 0 & 0 & 0 \\ \frac{s_2}{C_2} & 0 & \frac{1}{C_2} & 0 & 0 \end{bmatrix}, \tag{2}$$

the state vector is

$$x = [i \quad i_1 \quad i_2 \quad v_1 \quad v_2]^T, \tag{3}$$

the input is

$$f = \left[0 \quad \frac{V_1}{L_1} \quad -\frac{V_2}{L_2} \quad 0 \quad 0 \right]^T, \tag{4}$$

and the switching functions s_1, s_2 are

$$s_1(t) = \frac{1}{2} \left\{ \text{sgn} \left[\sin \left(\omega t + \frac{\phi_1}{2} \right) \right] - \text{sgn} \left[\sin \left(\omega t - \frac{\phi_1}{2} \right) \right] \right\}, \tag{5}$$

$$s_2(t) = \frac{1}{2} \left\{ \text{sgn} \left[\sin \left(\omega t - \phi_3 + \frac{\phi_2}{2} \right) \right] - \text{sgn} \left[\sin \left(\omega t - \phi_3 - \frac{\phi_2}{2} \right) \right] \right\}, \tag{6}$$

where the ω will denote the angular switching frequency. Moreover, it may be noted that the (5) and (6) depend on the three phase-shifts and expresses mathematically the shape of the v_{t1} and v_{t2} shown in Figure 2.

2.2. Generalized Average Modeling

The idea of the Generalized Average Modeling method is described in [13]. This approach is based on expanding state-equations of a given converter circuit into a Fourier series and deriving the differential equation governing the evolution of complex magnitudes of consecutive harmonics of each state variable. Choosing the number of harmonics for a particular state variable is arbitrary; however, the accuracy of this approach grows with the number of harmonics involved. The state space model with harmonic magnitudes as state variables facilitates the simulation and analysis of resonant, quasi-resonant topologies. This is also an effective way to analyze classic DC/DC converters where small ripple approximation is not assured [13]. On the other hand, this approach is general enough to encompass the small ripple modeling as a particular case, namely when only DC components of the Fourier expansion are taken into account. Furthermore, this approach allows for a calculation of harmonics content in given state variables and their time-domain waveform reconstruction. Finally, some implicit features such as power characteristics or converter efficiency may be easily calculated.

2.3. GAM Approach for the DAB

We can rewrite (1)–(4) in the form which is more convenient for further harmonic analysis, namely

$$\dot{x} = (A + s_1 B_1 + s_2 B_2 + s_1^2 B_3 + s_2^2 B_4)x + f, \tag{7}$$

where

$$A = \begin{bmatrix} -\frac{R}{L} & 0 & 0 & 0 & 0 \\ 0 & -\frac{(R_1+r_1)}{L_1} & 0 & -\frac{1}{L_1} & 0 \\ 0 & 0 & -\frac{(R_2+r_2)}{L_2} & 0 & -\frac{1}{L_2} \\ 0 & \frac{1}{C_1} & 0 & 0 & 0 \\ 0 & 0 & \frac{1}{C_2} & 0 & 0 \end{bmatrix}, \tag{8}$$

and B_1, B_2, B_3, B_4 are the 5×5 matrices, with

$$(B_1)_{1,2} = \frac{nr_1}{L}, \quad (B_1)_{2,1} = -\frac{nr_1}{L_1}, \tag{9}$$

$$(B_1)_{1,4} = \frac{n}{L}, \quad (B_1)_{4,1} = -\frac{n}{C_1}, \tag{10}$$

$$(B_2)_{1,3} = -\frac{r_2}{L}, \quad (B_2)_{3,1} = -\frac{r_2}{L_2}, \tag{11}$$

$$(B_2)_{1,5} = -\frac{1}{L}, \quad (B_2)_{5,1} = \frac{1}{C_2}, \tag{12}$$

$$(B_3)_{1,1} = -\frac{n^2 r_1}{L}, \quad (B_4)_{1,1} = -\frac{r_2}{L}, \tag{13}$$

and all remaining entries are equal to zero. Denoting

$$u_1 = s_1, \quad u_2 = s_2, \quad u_3 = s_1^2, \quad u_4 = s_2^2, \tag{14}$$

we can rewrite (7) as

$$\dot{x} = (A + \sum_{m=1}^4 u_m B_m)x + f. \tag{15}$$

Let us recall that the angular switching frequency is ω , and expand x and $u_m, m = 1, 2, 3, 4$, into complex trigonometric series

$$x = \sum_{k=-\infty}^{\infty} \langle x \rangle_k e^{ik\omega t}, \tag{16}$$

and

$$u_m = \sum_{k=-\infty}^{\infty} \langle u_m \rangle_k e^{ik\omega t}. \tag{17}$$

The Fourier coefficients of switching signals u_1, u_2, u_3, u_4 are given in the Appendix. From now on, we will use lighter notation and write \sum_k instead of $\sum_{k=-\infty}^{\infty}$. From (16) we get

$$\dot{x} = \sum_k \left(\frac{d}{dt} \langle x \rangle_k + ik\omega \langle x \rangle_k \right) e^{ik\omega t}. \tag{18}$$

Now substituting (16) and (18) into (15) we obtain

$$\sum_k \left(\frac{d}{dt} \langle x \rangle_k + ik\omega \langle x \rangle_k \right) e^{ik\omega t} = \left[A + \sum_{m=1}^4 \left(\sum_k \langle u_m \rangle_k e^{ik\omega t} \right) B_m \right] \sum_k \langle x \rangle_k e^{ik\omega t} + f \tag{19}$$

Arranging and equating the terms with respect to the powers of $e^{i\omega t}$ we obtain

$$\frac{d}{dt} \langle x \rangle_0 = A \langle x \rangle_0 + \sum_{m=1}^4 \left[B_m \sum_i \langle x \rangle_i \langle u_m \rangle_{-i} \right] + f \tag{20}$$

for $k = 0$ and

$$\frac{d}{dt} \langle x \rangle_k = (A - ik\omega I) \langle x \rangle_k + \sum_{m=1}^4 \left[B_m \sum_i \langle x \rangle_{k+i} \langle u_m \rangle_{-i} \right] \tag{21}$$

for $k \neq 0$. The range of indexes k, i in (20) and (21) is from $-\infty$ to ∞ . It is known from the theory of Fourier series that the Fourier coefficients tend to zero for $k \rightarrow \infty$, where k denotes the coefficient's index [20,21]. With this in mind, let us now make the following approximation, namely, that the range of indexes is from $-2N$ to $2N$, in other words, that the contribution of terms with higher indexes, that is, outside of the considered range, is negligible. With this truncation of index range, we can write (20) and (21) concisely in matrix form as

$$\frac{d}{dt} \mathbf{x} = \mathbf{A} \mathbf{x} + \mathbf{b} \tag{22}$$

where

$$\mathbf{x} = \begin{bmatrix} \langle x \rangle_{-N} \\ \langle x \rangle_{-N+1} \\ \vdots \\ \langle x \rangle_{-1} \\ \langle x \rangle_0 \\ \langle x \rangle_1 \\ \vdots \\ \langle x \rangle_{N-1} \\ \langle x \rangle_N \end{bmatrix}, \quad \mathbf{b} = \begin{bmatrix} 0 \\ 0 \\ \vdots \\ 0 \\ f \\ 0 \\ \vdots \\ 0 \\ 0 \end{bmatrix}, \tag{23}$$

and the block matrix \mathbf{A} is

$$\mathbf{A} = \begin{bmatrix} A_{1,1} & \dots & A_{1,2N+1} \\ \vdots & \ddots & \vdots \\ A_{2N+1,1} & \dots & A_{2N+1,2N+1} \end{bmatrix} \tag{24}$$

with the block $A_{p,q} \in \mathbb{C}^{n \times n}$ given by

$$A_{p,q} = \begin{cases} \sum_{m=1}^4 B_m \langle u_m \rangle_0 + A + i(N+1-p)\omega & \text{for } p = q, \\ \sum_{m=1}^4 B_m \langle u_m \rangle_{p-q} & \text{for } p \neq q. \end{cases} \quad (25)$$

Steady-States Analysis

Equation (22), describes the evolution of Fourier coefficients, i.e., the complex magnitudes of successive harmonics of the state vector x from (3), and is known as harmonic-state-space (HSS) model [22]. It is a linear differential equation and the vector \mathbf{b} is constant; hence, if the switching frequency is constant, and all eigenvalues of matrix A have negative real parts, the steady state is

$$\mathbf{x}_{ss} = \lim_{t \rightarrow \infty} \mathbf{x}(t) = -\mathbf{A}^{-1}\mathbf{b}. \quad (26)$$

Thus, the power characteristics can be computed in a straightforward way, without resorting to model simulation, by applying (26) for different phase shifts of switching functions. Once the complex magnitudes of successive harmonics are known, the state vector's x time-domain waveforms may be readily retrieved from (16).

2.4. Models' Comparison

This section presents numerical validation of the developed GAM model (7)–(25) and analyzes its performance in comparison to the exact LTP model given by (1)–(6). The relevant DAB converter's parameters (for both simulation models and experimental devices) are given in Table A1. The steady-states for these two different models are obtained simply by numerical matrix inversions (GAM), and by performing a dynamic simulation with numerical ordinary differential equations solver (LTP) until the steady state is achieved.

2.4.1. Waveforms Reconstruction

Plotting time domain waveforms for a given state variable with the GAM approach may be performed by the utilization of the (16) with steady-states complex harmonics' magnitudes calculated from the (26). Figure 4 shows the transformer's alternating current where the gray color corresponds to the DAB LTP state-space model and is compared to the appropriate reconstructions obtained for the GAM approach with harmonics order up to: 1st, 3rd, 5th, and 21st. The test was done at voltage levels $V_1 = 270$ V and $V_2 = 200$ V for the TPS with $\phi_1 = \phi_2 = \pi/2$, $\phi_3 = -\pi/4$ to challenge the method by forcing it to consider the higher order models with higher transformer's current harmonics; such currents occur in DAB with phase shifts ϕ_1 and ϕ_2 lower than π as well as with V_2/V_1 ratios different than 1.

2.4.2. Power Characteristics

Figure 5 shows the power input/output (i.e., the P_1 , P_2) characteristics family referred to ϕ_3 phase-shift and obtained for given voltages V_1 , V_2 and ϕ_1 , ϕ_2 of the TPS conditions. It shows the comparison between results simulated with the DAB LTP model (gray dashed and solid lines for P_1 and P_2 , respectively) and the GAM models calculated for a different number of successive harmonics (1st, 3rd, 5th). The P_1 and P_2 powers may be calculated as product of constant values of supplying DC-link voltages V_1 and V_2 with their corresponding i_1 , i_2 current values obtained from (26) and their successive harmonic amplitudes' RMS values.

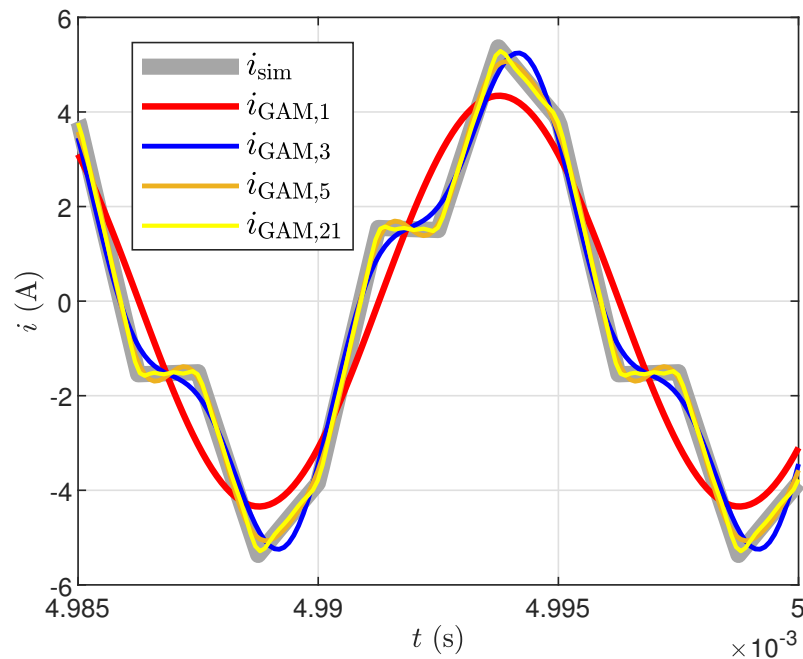


Figure 4. Transformer’s current harmonics reconstruction with different model order for the TPS modulation (color lines) referred to the LTP model ODE simulation (gray).

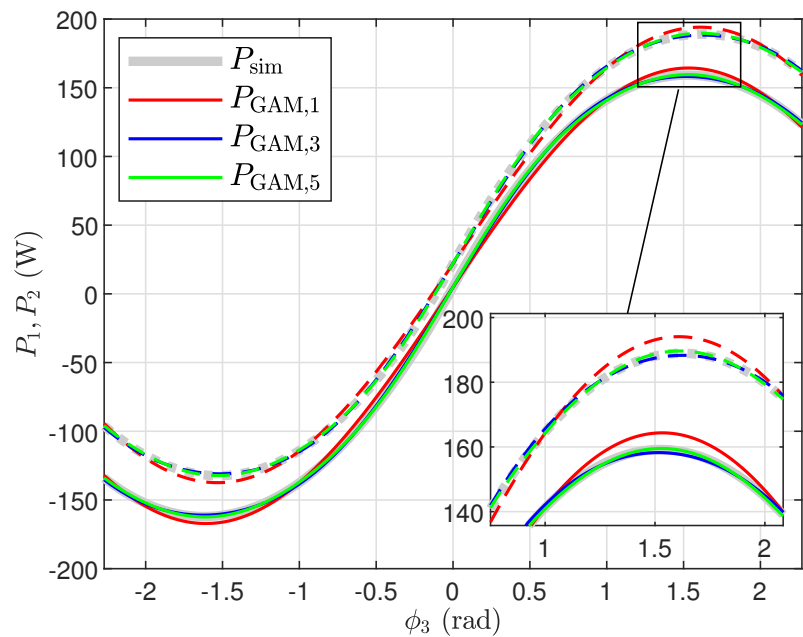


Figure 5. DAB converter’s P_1, P_2 (dashed and solid lines, respectively) power curves comparison. Gray color lines correspond to simulated LTP model; the GAM approach is depicted with color lines for models of different orders.

These simulations and analyses were done for circuit conditions as follows: $V_1 = 270$ V, $V_2 = 60$ V, $\phi_1 = \phi_2 = \pi/2$, which challenged the method again with highly distorted transformer’s current. The differences between particular model harmonics’ order may be better grasped with the help of the picture-in-picture in Figure 5. It may be noted that ϕ_3 angle is validated in a range of $\pm 5/7\pi$ which is beyond practical utilization because maximum power values occur at $\pm \pi/2$. Nonetheless, with the presented range again, a significant current higher harmonics occur and this allows us to verify the method even more.

The presented results show that the GAM model of the DAB converter equivalent circuit performs very well, and that it demonstrates a satisfying accuracy even when a relatively low number of Fourier harmonics are taken into account (e.g., 3rd or 5th order).

3. Results

3.1. Lab Setup

To verify an accuracy of the proposed GAM method for the DAB converter, a laboratory setup was designed and its general scheme is depicted in Figure 6.

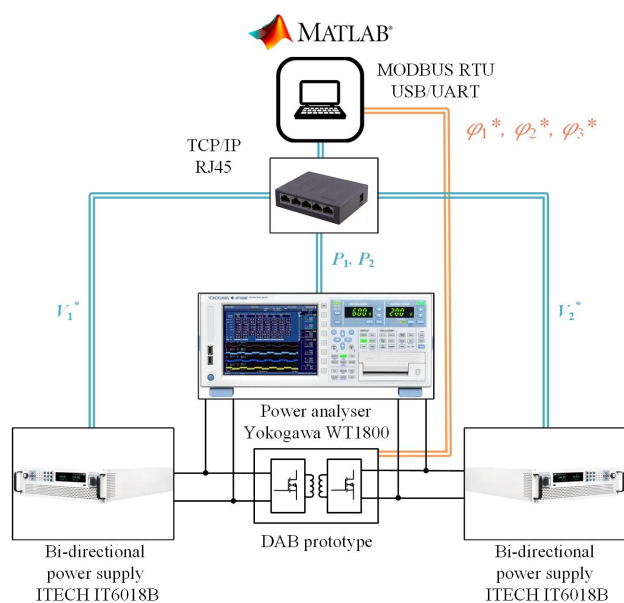


Figure 6. Laboratory setup block diagram.

The examined converter is located at the bottom of the block diagram. Both of its DC circuits are connected to bi-directional laboratory power supplies ITECH IT6018B. Thanks to this connection the energy transfer in both directions is assured as well as a simple change in the voltage levels that may emulate, e.g., a battery voltage drop due to discharging processes. Every single H-bridge of the DAB converter consists of 8 C3M0065090J SiC MOSFET transistors with rated MOSFET resistance of 65 m Ω each; hence, each logic switch is composed of two parallel MOSFETs in order to achieve lower overall channel resistance, which improves the device's total efficiency. Similarly, the external STPSC6H065 freewheeling diode was used in parallel to every switch to reduce transistors' intrinsic SiC body diode voltage drop from 4.4 V to 1.56 V. The auxiliary inductance equals $L' = 62 \mu\text{H}$. A complete list of the DAB converter prototype parameters are listed in Table A1 and the converter itself is shown in Figure 7.

Measurements of DC power, current and voltage are performed by YOKOGAWA WT1800 power analyser using two isolated channels—one for each of the DC-links.

In order to automate the measurement process and to shorten the duration of repetitive experiments, all the devices are connected to a PC via specified interfaces and the proper communication protocols. The PC acts as a master device and executes scenarios written by a user in MathWorks MATLAB script. The three phase-shift values (ϕ_1 , ϕ_2 , ϕ_3) are sent from the PC via MODBUS RTU protocol to the converter's TMS320F28379D microcontroller, where proper gate signals of the DAB transistors are generated. Subsequently, the required measurements such as DC-links powers, voltages, and currents are sent back via TCP/IP on the PC demand. Additionally, the Tektronix MDO34 oscilloscope was used to observe transformer current and voltage waveforms. The experimental procedure may then be simply repeated in a loop for different values of phase-shifts and DC voltages. The elaborated laboratory setup is depicted in Figure 8.

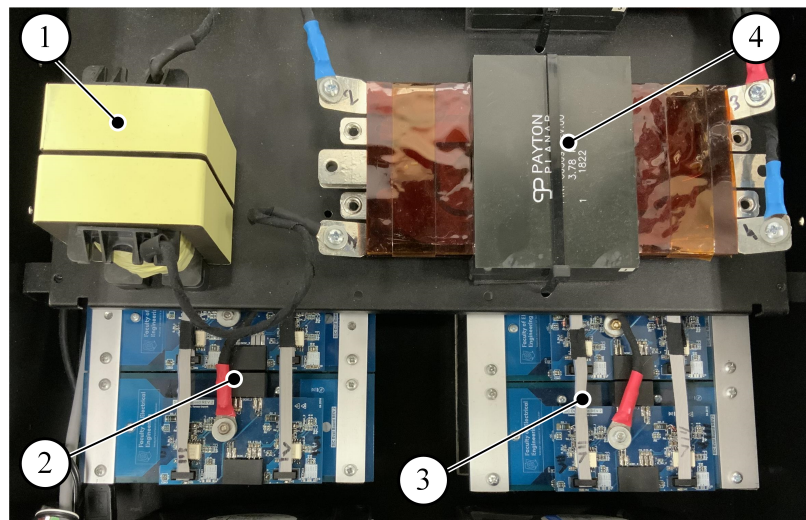


Figure 7. 1.5 kW, 100 kHz DAB prototype: 1—auxiliary inductance, 2–3—SiC based H-Bridges, 4—high-frequency planar transformer.

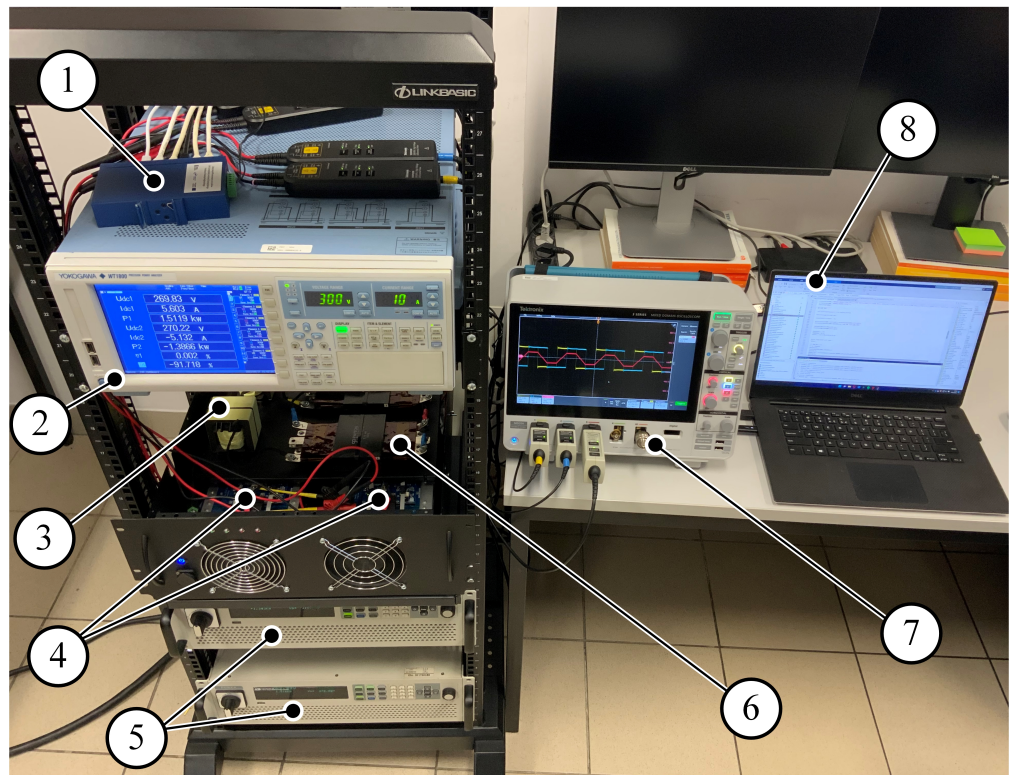


Figure 8. Laboratory setup, where 1—ethernet switch, 2—power analyser, 3—auxiliary leakage inductance, 4—H-bridges, 5—power supplies, 6—HF transformer, 7—oscilloscope, 8—PC with Matlab software.

3.2. Results Comparison

3.2.1. Waveform Reconstruction

The accuracy of the proposed approach may be validated by comparing measured waveforms (especially the transformer's current due to its higher harmonics content) with their reconstructed analytical counterparts. The results conducted for the transformer's current reconstruction are shown in Figure 9 and were performed for two completely different operating conditions to prove versatility of the method. Figure 9a considers conditions where $\phi_1 = \phi_2 = \pi$ (SPS) and $\phi_3 = \pi/2$ for $V_1 = V_2 = 270$ V, whereas

Figure 9b shows a case of TPS with $\phi_1 = \phi_2 = \pi/2$ and $\phi_3 = -\pi/4$ for $V_1 = 270$ V and $V_2 = 200$ V. In each case, the upper panels present experimental test-bench transformer voltages v_{t1} and v_{t2} , and the bottom ones display the experimental transformer's current waveform (gray color) compared with the 3rd and 5th order of the GAM model waveform reconstruction, denoted with blue and green colors, respectively.

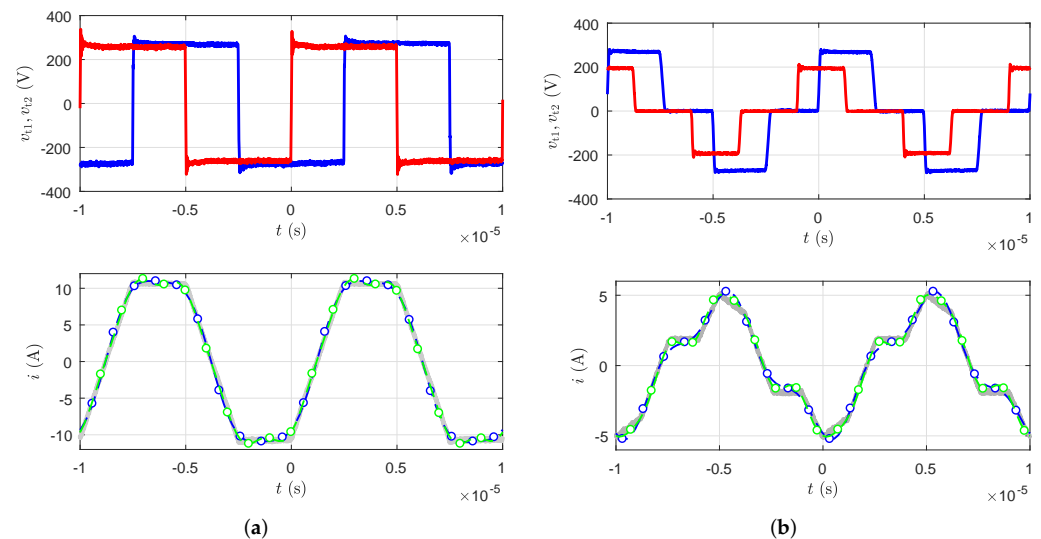


Figure 9. Experimental validation of the GAM current reconstruction with GAM approach. The top panel shows the DAB transformer v_{t1} and v_{t2} measured voltages (blue and red, respectively); the bottom panel presents measured experimental i current (gray color) with 3rd (dashed blue), and 5th (dashed green) order models of the GAM method for the following conditions: (a) SPS for $\phi_1 = \phi_2 = \pi$, $\phi_3 = \pi/2$, $V_1 = 270$ V, $V_2 = 270$ V, (b) TPS $\phi_1 = \phi_2 = \pi/2$, $\phi_3 = -\pi/4$ for $V_1 = 270$ V, $V_2 = 200$ V.

3.2.2. Power Characteristics

This test verifies the proposed model for a wider spectrum of operating conditions due to drawing steady-state power characteristics.

Figure 10 shows a comparison between the experimental data and the curves calculated from the analytical GAM model. The following comparison was made for the SPS modulation (i.e., $\phi_1 = \phi_2 = \pi$) with the GAM model extended up to the 5th harmonic and conducted for two different voltage conditions: Figure 10a corresponds to $V_1 = 270$ V, and $V_2 = 180$ V, whereas, Figure 10b corresponds to $V_1 = 270$ V, and $V_2 = 60$ V. It is important to mention that the experimental data (i.e., P_1 and P_2 denoted with red and blue color markers, respectively) are measured with $\pi/36$ radians resolution; however, the markers are placed less dense for the sake of clarity. Furthermore, the solid gray line corresponds to P_1 characteristics obtained directly from the GAM model; a similar line may be plotted for the P_2 power; however, for the sake of clarity, it was omitted. It is clear that the measured P_1 power curve matches with good accuracy the gray line characteristics for $\phi_3 > \pi/2$ and $\phi_3 < -\pi/2$; however, it differs slightly in the range between these values. This is the effect called phase-shift-drift (with its value denoted as θ_{DT}) and has been described, e.g., in [23]. It is caused by the dead-time of switching transistors and depends on the operating conditions such as the V_1 , V_2 voltages ratio as well as on the ϕ_3 value. Thus, the red and blue solid continuous lines are the GAM model P_1 and P_2 power curves with an applied constant phase-shift-drift correction factor, which was introduced according to the method presented in [5] and was similarly applied in [17]. This factor may be expressed by $\theta_{DT} = \omega \cdot DT$ relationship.

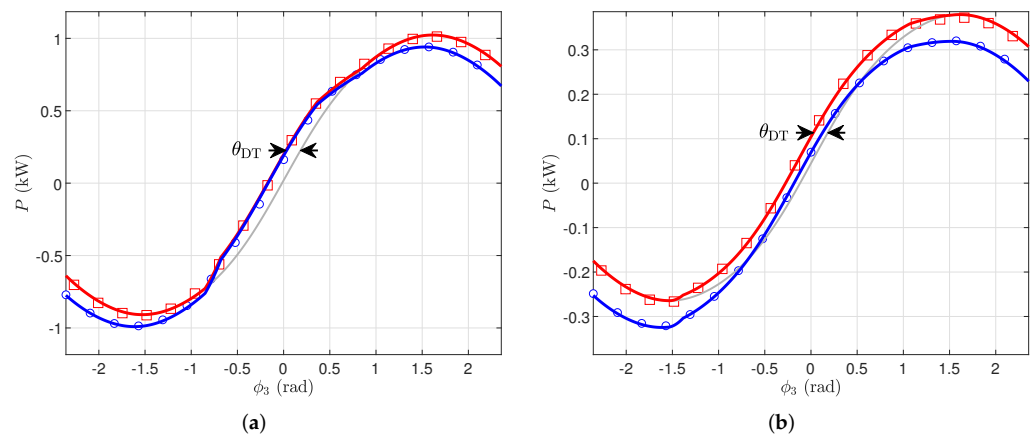


Figure 10. Comparison between experimental P_1 , P_2 (square and circle, respectively) power characteristics with 5th order GAM model characteristics without (gray color) and with (red and blue, respectively) dead-time phase-drift correction factor, for two different SPS ($\phi_1 = \phi_2 = \pi$) cases: (a) $V_1 = 270$ V, $V_2 = 180$ V (b) $V_1 = 270$ V, $V_2 = 60$ V.

Finally, Figure 11 presents experimental validation for the TPS ($\phi_1 = \phi_2 = \pi/2$ in this case) conducted with voltages $V_1 = 270$ V and $V_2 = 180$ V (Figure 11a) and $V_1 = 270$ V and $V_2 = 60$ V (Figure 11b). Here, it may be noticed that, due to the TPS, the maximum power for the same conditions as for SPS is lowered, which is obvious as the voltage waveform with some zero levels has lower RMS values than typical 2-level square-waves. However, some differences between experimental data and the GAM model results are more visible now. The solid lines are now solely obtained from the GAM method without any correction factor. It may be observed that even if the GAM calculated power characteristics give similar values to the experiment, they are slightly shifted. As the simulation results presented in Figure 5 of the previous section show, the method works in good agreement, although the GAM model does not include dead-time effect. The simple correction factor does not work here because with the TPS an additional phase-shift drift effects occur. Thus, it cannot be simply corrected like the one in the previous case, and requires further studies.

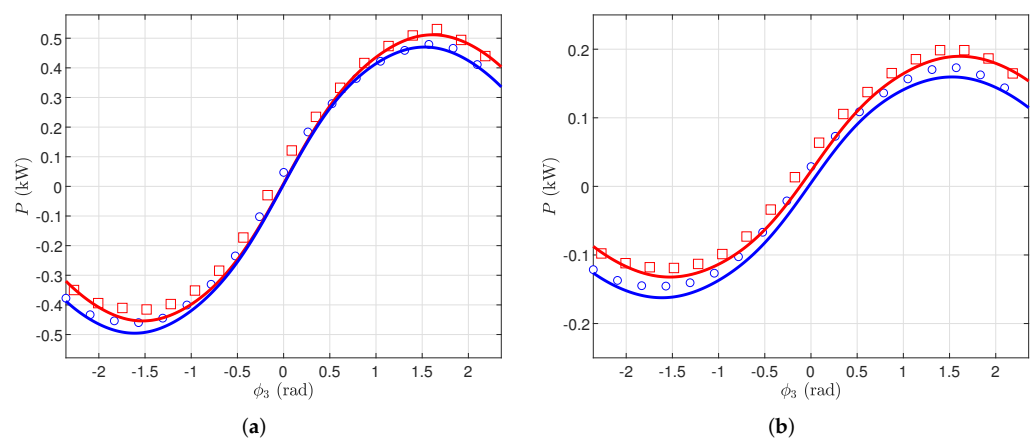


Figure 11. Comparison between experimental P_1 , P_2 (square and circle, respectively) power characteristics with 5th order GAM model characteristics without (red and blue, respectively) dead-time phase-drift correction factor, for two different TPS ($\phi_1 = \phi_2 = \pi/2$) cases: (a) $V_1 = 270$ V, $V_2 = 180$ V (b) $V_1 = 270$ V, $V_2 = 60$ V.

4. Conclusions

The modeling approach presented in this paper describes the DAB converter with a coherent electrical equivalent circuit along with a rigorously defined Triple Phase Shift

modulation. Simple and fast steady-states calculations for a wide range of operating conditions constitute the main advantage of this model. This may be done by numerical matrix inversion without resorting to tedious simulations with a use of ODE solvers. The proposed method offers a deep insight into the harmonic content of virtually any system variable; the high-frequency transformer current being in focus as one of the most important and challenging variables. This information may be especially important in the process of DAB high-frequency transformer or auxiliary inductor design. Additionally, the time waveforms may be readily reconstructed if needed. Finally, the discussed approach allows for DAB power characteristics calculation based only on steady-state magnitudes of the GAM model. Relatively low harmonic order is required to model the converter accurately, even for high DC voltages ratios and for different conditions of the Triple Phase-Shift modulation. The presented results demonstrate a very good agreement of the model with the experiments.

Author Contributions: Data curation, M.R. and C.S.; Formal analysis, M.T.; Funding acquisition, M.R.; Investigation, M.R., M.T. and C.S.; Methodology, M.T. and C.S.; Project administration, M.R.; Resources, M.R. and M.T.; Software, M.T. and C.S.; Supervision, M.R.; Validation, M.R., M.T. and C.S.; Visualization, M.R. and C.S.; Writing—original draft, M.R., M.T. and C.S.; Writing—review & editing, M.R., M.T. and C.S. All authors have read and agreed to the published version of the manuscript.

Funding: Studies were funded by ENERGYTECH-1 project granted by Warsaw University of Technology under the program Excellence Initiative: Research University (ID-UB).

Institutional Review Board Statement: Not applicable.

Informed Consent Statement: Not applicable.

Data Availability Statement: Not applicable.

Conflicts of Interest: The authors declare no conflict of interest.

Abbreviations

The following abbreviations are used in this manuscript:

DAB	Dual Active Bridge
SPS	Single Phase Shift modulation
TPS	Triple Phase Shift modulation
LTP	linear-time-periodic
GAM	General Average Modeling
ODE	Ordinary Differential Equation
ESR	Equivalent Series Resistance

Appendix A. Fourier Expansions of Switching Signals

In order to complete the Fourier description of the model we consider, we have to determine the Fourier coefficients of switching signals (14), namely, u_1 , u_2 , u_3 , u_4 . From general theory of Fourier series [20,21] we know that a periodic signal $u(t)$ with period $T = 2\pi/\omega$ can be expressed as

$$u(t) = \sum_{k=-\infty}^{\infty} \langle u \rangle_k e^{ik\omega t} \quad (\text{A1})$$

where

$$\langle u \rangle_k = \frac{1}{T} \int_0^T u(t) e^{-ik\omega t} dt. \quad (\text{A2})$$

For real signals this implies $\langle u \rangle_k = \langle u \rangle_{-k}^*$, i.e., $\langle u \rangle_k$ equals the complex conjugate of $\langle u \rangle_{-k}$. Now, taking into account (5), (6) and (14), we obtain

$$\langle u_1 \rangle_k = \begin{cases} 0 & \text{for } k = 2n, \\ \frac{2}{k\pi} \sin\left(\frac{k\phi_1}{2}\right) e^{-\frac{ik\phi_1}{2}} & \text{for } k = 2n + 1, \end{cases} \quad (\text{A3})$$

$$\langle u_2 \rangle_k = \begin{cases} 0 & \text{for } k = 2n, \\ \frac{2}{k\pi} \sin\left(\frac{k\phi_2}{2}\right) e^{-ik\left(\frac{\phi_2}{2} + \phi_3\right)} & \text{for } k = 2n + 1, \end{cases} \quad (\text{A4})$$

$$\langle u_3 \rangle_k = \begin{cases} \frac{\phi_1}{\pi} & \text{for } k = 0, \\ 0 & \text{for } k = 2n + 1, \\ \frac{2}{k\pi} \sin\left(\frac{k\phi_1}{2}\right) e^{-\frac{ik\phi_1}{2}} & \text{for } k = 2n \neq 0, \end{cases} \quad (\text{A5})$$

$$\langle u_4 \rangle_k = \begin{cases} \frac{\phi_2}{\pi} & \text{for } k = 0, \\ 0 & \text{for } k = 2n + 1, \\ \frac{2}{k\pi} \sin\left(\frac{k\phi_2}{2}\right) e^{-ik\left(\frac{\phi_2}{2} + \phi_3\right)} & \text{for } k = 2n \neq 0, \end{cases} \quad (\text{A6})$$

Table A1. Simulation and Experimental DAB's Parameters.

Parameter	Symbol	Value	Unit
DAB max. power	P_{\max}	1500	W
HV voltage	V_1	270	V
Energy Storage voltage range	V_2	60 to 270	V
Switching frequency	f	100	kHz
Auxiliary inductance	L'	62	μH
Lumped inductance	L	63	μH
Windings' lumped resistance	R'	14	$\text{m}\Omega$
Total lumped resistance	R	1.5	Ω
Dead-time	DT	250	ns
Transformer winding ratio	n	1:1	(-)
MOSFET's gate resistor	R_g	4	Ω
DC-links capacity	C_1, C_2	1.5	mF
DC-links ESRs	r_1, r_2	5	$\text{m}\Omega$
input/output inductance	L_1, L_2	2.45	μH
input/output inductance's resistance	R_1, R_2	10	$\text{m}\Omega$
MOSFET's channel resistance	$R_{\text{DS,ON}}$	65	$\text{m}\Omega$

References

- Liu, T.; Yang, X.; Chen, W.; Xuan, Y.; Li, Y.; Huang, L.; Hao, X. High-Efficiency Control Strategy for 10-kV/1-MW Solid-State Transformer in PV Application. *IEEE Trans. Power Electron.* **2020**, *35*, 11770–11782. [CrossRef]
- Zhao, B.; Song, Q.; Liu, W.; Sun, Y. Overview of dual-active-bridge isolated bidirectional DC-DC converter for high-frequency-link power-conversion system. *IEEE Trans. Power Electron.* **2014**, *29*, 4091–4106. [CrossRef]
- Shao, S.; Chen, L.; Shan, Z.; Gao, F.; Chen, H.; Sha, D.; Member, S.; Dragičević, T. Modeling and Advanced Control of Dual-Active-Bridge DC-DC Converters: A Review. *IEEE Trans. Power Electron.* **2022**, *37*, 1524–1547. [CrossRef]
- Doncker, W.A.A.D.; Divan, D.M. A Three-phase Soft-Switched High-Power-Density dc/dc Converter for High-Power Applications. *IEEE Trans. Ind. Appl.* **1991**, *27*, 63–73. [CrossRef]
- Segaran, D.; Holmes, D.G.; McGrath, B.P. Enhanced load step response for a bidirectional DCDC converter. *IEEE Trans. Power Electron.* **2013**, *28*, 371–379. [CrossRef]
- Song, W.; Hou, N.; Wu, M. Virtual Direct Power Control Scheme of Dual Active Bridge DC-DC Converters for Fast Dynamic Response. *IEEE Trans. Power Electron.* **2018**, *33*, 1750–1759. [CrossRef]
- Gierczynski, M.; Grzesiak, L.M.; Kaszewski, A. A dual rising edge shift algorithm for eliminating the transient dc-bias current in transformer for a dual active bridge converter. *Energies* **2021**, *14*, 4264. [CrossRef]
- Choi, W.; Lee, M.; Cho, B.H. Fundamental Duty Modulation of Dual-Active-Bridge Converter for Wide-Range Operation. *IEEE Trans. Power Electron.* **2016**, *31*, 1416–1423. [CrossRef]

9. Tong, A.; Hang, L.; Li, G.; Huang, J. Nonlinear characteristics of DAB converter and linearized control method. In Proceedings of the IEEE Applied Power Electronics Conference and Exposition—APEC, San Antonio, TX, USA, 4–8 March 2018; pp. 331–337. [[CrossRef](#)]
10. Gu, Q.; Yuan, L.; Nie, J.; Sun, J.; Zhao, Z. Current Stress Minimization of Dual-Active-Bridge DC-DC Converter within the Whole Operating Range. *IEEE J. Emerg. Sel. Top. Power Electron.* **2019**, *7*, 129–142. [[CrossRef](#)]
11. Rolak, M.; Sobol, C.; Malinowski, M.; Stynski, S. Efficiency Optimization of Two Dual Active Bridge Converters Operating in Parallel. *IEEE Trans. Power Electron.* **2020**, *35*, 6523–6532. [[CrossRef](#)]
12. Erickson, R.W.; Maksimovic, D. *Fundamentals of Power Electronics*, 2nd ed.; Springer Science+Business Media, LLC: Berlin/Heidelberg, Germany, 2001; pp. 1–881. [[CrossRef](#)]
13. Sanders, S.R.; Noworolski, J.M.; Liu, X.Z.; Verghese, G.C. Generalized Averaging Method for Power Conversion Circuits. *IEEE Trans. Power Electron.* **1991**, *6*, 251–259. [[CrossRef](#)]
14. Erni, I.R.; Vidal-Idiarte, E.; Calvente, J.; Guasch-Pesquer, L. Small Signal Modelling for Variable Frequency Control with Maximum Efficiency Point Tracking of DAB Converter. *IEEE Access* **2021**, *9*, 85289–85299. [[CrossRef](#)]
15. Shah, S.S.; Bhattacharya, S. Large & small signal modeling of dual active bridge converter using improved first harmonic approximation. In Proceedings of the IEEE Applied Power Electronics Conference and Exposition—APEC, Tampa, FL, USA, 26–30 March 2017; pp. 1175–1182. [[CrossRef](#)]
16. Uicich, S.; Gauthier, J.Y.; Lin-Shi, X.; Allard, B.; Plat, A. General DAB 1stHarmonic TPS State Space Model. In Proceedings of the IECON 2021—47th Annual Conference of the IEEE Industrial Electronics Society, Toronto, ON, Canada, 13–16 October 2021. [[CrossRef](#)]
17. Mueller, J.A.; Kimball, J.W. An Improved Generalized Average Model of DC-DC Dual Active Bridge Converters. *IEEE Trans. Power Electron.* **2018**, *33*, 9975–9988. [[CrossRef](#)]
18. Cupelli, M.; Member, S.; Gurumurthy, S.K.; Monti, A.; Member, S. Modelling and Control of Single Phase DAB based MVDC Shipboard Power System Institute for Automation of Complex Power Systems. In Proceedings of the IECON 2017—43rd Annual Conference of the IEEE Industrial Electronics Society, Beijing, China, 29 October–1 November 2017; Volume 1, pp. 6813–6819.
19. Bhattacharjee, A.; Batarseh, I. A PI Based Simplified Closed Loop Controller for Dual Active Bridge DC-AC Converter for Standalone Applications. In Proceedings of the 2020 IEEE Applied Power Electronics Conference and Exposition (APEC), New Orleans, LA, USA, 15–19 March 2020.
20. Zygmund, A. *Trigonometrical Series*; Dover Publications: New York, NY, USA, 1955.
21. Tolstov, G. *Fourier Series*; Dover Publications: New York, NY, USA, 2012.
22. Lin, J.; Su, M.; Sun, Y.; Li, X.; Xie, S.; Zhang, G.; Blaabjerg, F.; Feng, J. Accurate Loop Gain Modeling of Digitally Controlled Buck Converters. *IEEE Trans. Ind. Electron.* **2022**, *69*, 725–739. [[CrossRef](#)]
23. Takagi, K.; Fujita, H. *Dynamic Control and Dead-Time Compensation Method of an Isolated Dual-Active-Bridge DC-DC Converter*. In Proceedings of the 2015 17th European Conference on Power Electronics and Applications (EPE'15 ECCE-Europe), Geneva, Switzerland, 8–10 September 2015. [[CrossRef](#)]